Molecular Diversity
https://doi.org/10.1007/s11030-022-10405-9

ORIGINAL ARTICLE

Defective ORF8 dimerization in SARS-CoV-2 delta variant leads to a better adaptive immune response due to abrogation of ORF8-MHC1 interaction

Armi M. Chaudhari[1] · Indra Singh[1] · Madhvi Joshi[1] · Amrutlal Patel[1] · Chaitanya Joshi[1]

Received: 25 November 2021 / Accepted: 8 February 2022

Abstract

In India, during the second wave of the COVID-19 pandemic, the breakthrough infections were mainly caused by the SARS-COV-2 delta variant (B.1.617.2). It was reported that, among majority of the infections due to the delta variant, only 9.8% percent cases required hospitalization, whereas only 0.4% fatality was observed. Sudden dropdown in COVID-19 infections cases were observed within a short timeframe, suggesting better host adaptation with evolved delta variant. Downregulation of host immune response against SARS-CoV-2 by ORF8 induced MHC-I degradation has been reported earlier. The Delta variant carried mutations (deletion) at Asp119 and Phe120 amino acids which are critical for ORF8 dimerization. The deletions of amino acids Asp119 and Phe120 in ORF8 of delta variant resulted in structural instability of ORF8 dimer caused by disruption of hydrogen bonds and salt bridges as revealed by structural analysis and MD simulation studies. Further, flexible docking of wild type and mutant ORF8 dimer revealed reduced interaction of mutant ORF8 dimer with MHC-I as compared to wild-type ORF8 dimer with MHC-1, thus implicating its possible role in MHC-I expression and host immune response against SARS-CoV-2. We thus propose that mutant ORF8 of SARS-CoV-2 delta variant may not be hindering the MHC-I expression thereby resulting in a better immune response against the SARS-CoV-2 delta variant, which partly explains the possible reason for sudden drop of SARS-CoV-2 infection rate in the second wave of SARS-CoV-2 predominated by delta variant in India.

Armi M. Chaudhari and Indra Singh authors are contributed equally to this work.

✉ Chaitanya Joshi
director@gbrc.res.in

[1] Gujarat Biotechnology Research Centre (GBRC), Department of Science and Technology, Government of Gujarat, 6th Floor, Block B&D, MS Building, Gandhinagar 382011, India

Published online: 03 March 2022

Graphical abstract

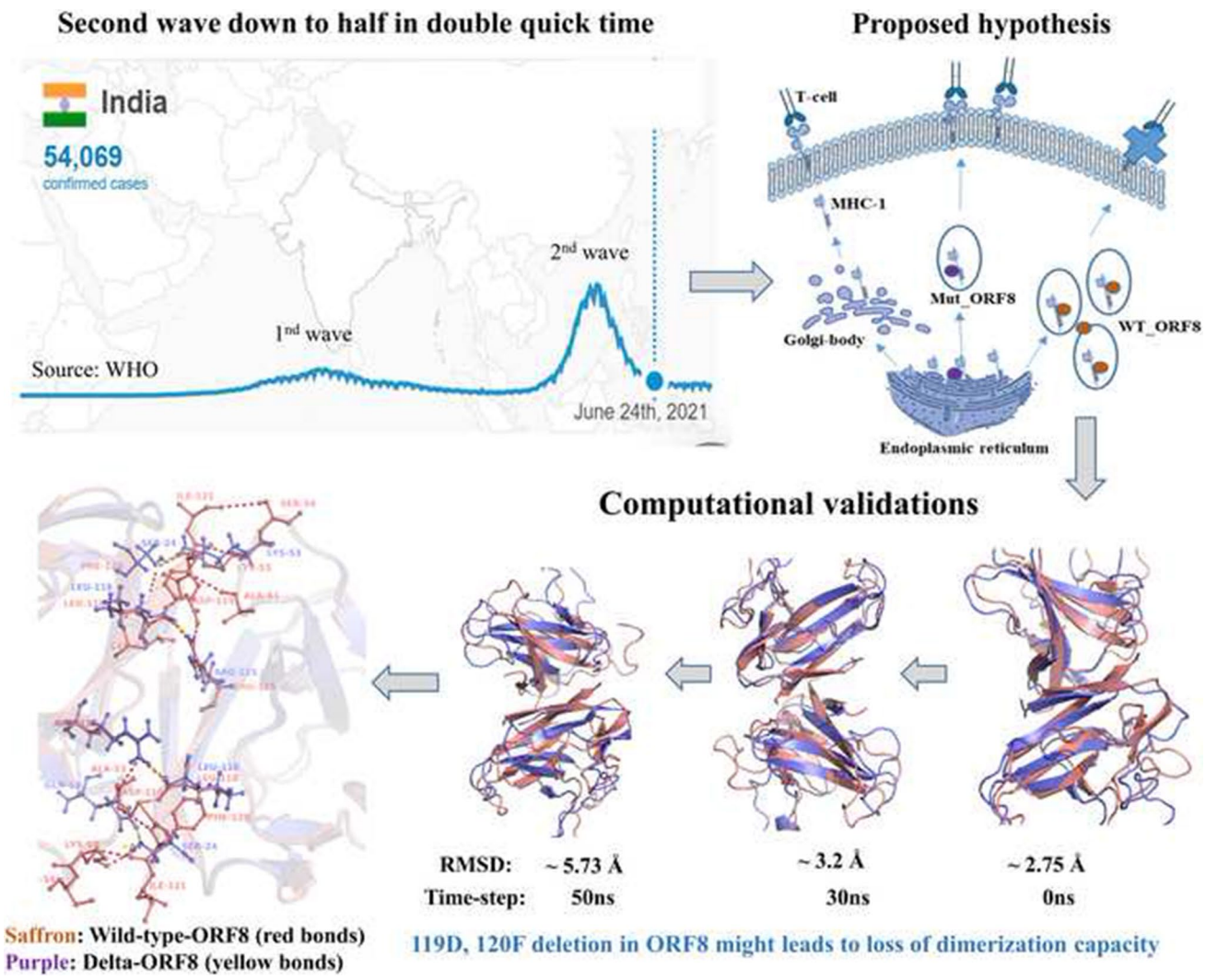

Keywords SARS-COV-2 · Delta variant · COVID-19 · MHC1 · ORF8 · Protein dimerization · Protein–protein interactions · MD simulations · Seroprevalence · Asp119 · Phe120 deletion

Introduction

Until 3 February 2022, the SARS-CoV-2 pandemic has infected over 380million people worldwide, resulting in almost 5.6 million deaths. There are many mutations occurs by chance in SARS-CoV-2 resulting in higher or lower transmissibility. Several research organizations used high throughput sequencing approaches to investigate the variations of SARS-CoV-2 and their influence on the host. With so many variants, the US government's SARS-CoV-2 Interagency Group (SIG) developed a variant classification method that divides SARS-CoV-2 variants into three categories: 1) VOI, 2) VOC, and 3) VOHC. During the second wave of infection in India, the delta variation of the VOCs group had experienced a rise in infection. This delta variant is seeming to be highly contagious due to mutations in spike as well as other regions of viral protein. Several other mutations like D614G in modulating higher spike infectivity and density, E484K for decreased antibody neutralization, N501Y and K417N for altering spike interacting with ACE receptor and antibodies derived from humans were reported [13, 17, 42]. There are several mutations which favors the host for example C241T, where viral replication efficiency with respect to host replication factors in decreased [8]. Recent reports suggest that NTD (N-Terminal Domain) is known to be supersite for antibody-mediated binding [10, 25, 33].

Reports on rigidization in NTD of spike had led to the antibody escape mechanism in this delta variant [9]. These studies are enough to display how lethal that this delta variant is in terms of transmittance, infectivity, and evading host immune responses.

In India, the second wave of Covid-19 was persisted from the middle of the March 2021, till June 2021 [40]. The preliminary focus of the current study lies in finding the possible reasons of the sudden drop down of the second wave of SARS-CoV-2 in the halved period as compared to the first wave with increased seroprevalence. India have 0.75% of seroprevalence in March 2021 during first wave which was drastically increased to 75–80% during second wave [26]. The virus genome is extensively studied and possible mutations favoring the host were identified using protein dynamics approach, among them ORF8 carrying mutations Δ119Asp and Δ120Phe had grabbed our attention due to their direct involvement in dimerization of ORF8 by forming hydrogen bonds and salt bridges [12]. The crystal structure of ORF8 was taken as a reference protein structure to study the effect of mutations/deletions using molecular modeling and simulation approach [12]. ORF8 is known to be an important protein for SARS-CoV-2 mediated infection by downregulation MHC-I molecule in ER (endoplasmic reticulum pathway) mediated protein trafficking pathway [44]. Involvement of ORF8 in endoplasmic reticulum mediated stress and antagonizing IF-beta (interferon beta) for immune evasion has also been studied [28]. Deletion of ORF8 leads to decreased severity of infection as reported [27, 46]. ORF8 is also involved in suppression antiviral proteins from INFγ [14]. SARS-CoV-2 drug or vaccines were using spike protein as an important target [20, 37, 38, 41], but ORF8 can be also targeted for producing therapeutic approaches. These studies shows that ORF8 is involved in modulating the host immune response and majorly by downregulating MHC-I. The exact interface of MHC-I binding with ORF8 is not known yet. In the current study, effect of Δ119Asp and Δ120Phe deletions concerning ORF8 dimerization has been studied extensively. ICMR report was also to correlating our findings for ORF8 function with second wave seroprevalence data. As previously discussed, ORF8 physically binds to the MHC-1 complex (confirmed using confocal microscopy), preventing its trafficking and membrane expression. ORF8 with Δ119Asp and Δ120Phe mutations loses its ability to form dimers because Asp and Phe are the major amino acids that are involved in the formation of hydrogen bonds between ORF8 dimers. If ORF8 becomes weak, it is no longer able to block MHC-1, and thus, normal ORF expression may occur in the host. Using a molecular dynamics approach, we investigated the possible reasons for loss of dimerization. Flexible induced docking was also performed to study the ORF8 mediated MHC-I binding. Mutations were correlated with a timeline of second wave and available cohort study on seroprevalence.

Results

Effect of deletions on the binding affinity of MUT_ ORF8 dimer

WT_ORF8 protein consists of two monomeric chains existing as a dimeric structure, tightly packed with the help of various electrostatic interactions and H-bonds (Supplementary figure S1). The key residues involved in the packing of WT_ORF8 dimers are Lys53, Arg115, Asp119, Phe120, and Ile121. Other residues involved in intrachain bonds between dimers of WT_ORF8 are Gln18, Ser24, Ala51, Arg52, and Ser54 (Fig. 1A). These dimers are closely held together with four salt bridges formed between A: Asp119-B: Arg115, A: Arg115-B: Glu92, B: Asp119-A: Arg115, and B: Arg115-A: Glu92. Other interactions are several other H-bonds formed between Phe120 and Lys53, Lys53 and Ser24, Gln18-Lue22, Arg52, and Ile121 (Fig. 1A). In WT_ORF8, amino acids Asp119 and Phe120 are predominantly involved in the formation of salt bridges as well as hydrogen bonds (Supplementary figure S1: C & D). The detailed analysis of MUT_ORF8 dimer protein showed that its monomer units are attached with only 1 salt bridge between C: Arg15-D: Glu92. Other six H-bonds are formed between amino acids C: Gln18-D: Ser24 (one H-bond), C: Arg115-D: Leu118 (two H-bonds), and C: Ile119-D: Ala51 (three H-bonds) (Supplementary figure S1: C & D). Protein structural interaction network analysis shows reduced nodes (amino acids) and bonds (edges). WT_ORF has 722 edges while Mut_ORF8 has only 714 (Fig. 1B). Decreased edges correlated with reduced protein–protein interactions (here in the case of monomers). These decreased monomeric interactions in MUT_ORF8 might leads to less stable dimer formation of ORF8. Ramachandran plot for both variants of simulated energy minimized dimers of ORF8 is shown in Fig. 1C. WT_ORF8 possesses the majority of amino acids in the highly preferred region (green) with no questionable interactions, while mutant ORF8 possess one questionable angles for amino acid C: E-64 (shown in red dots), depicting a decrease in protein stability of MUT_ORF8 (Fig. 1C). For WT_ORF8 amino acids falling in highly preferred region (green) while MUT_ORF8 have higher number of amino acids falling into moderate region (Fig. 1C). Contact plot generated for inter and intramolecular interactions within ORF8 dimers where WT_ORF8 possesses higher inter-intramolecular interactions compared to MUT_ORF8 and leads to more stable dimer (Fig. 1D). Circle highlighting higher interactions in WT_ORF8 is significantly higher compare to

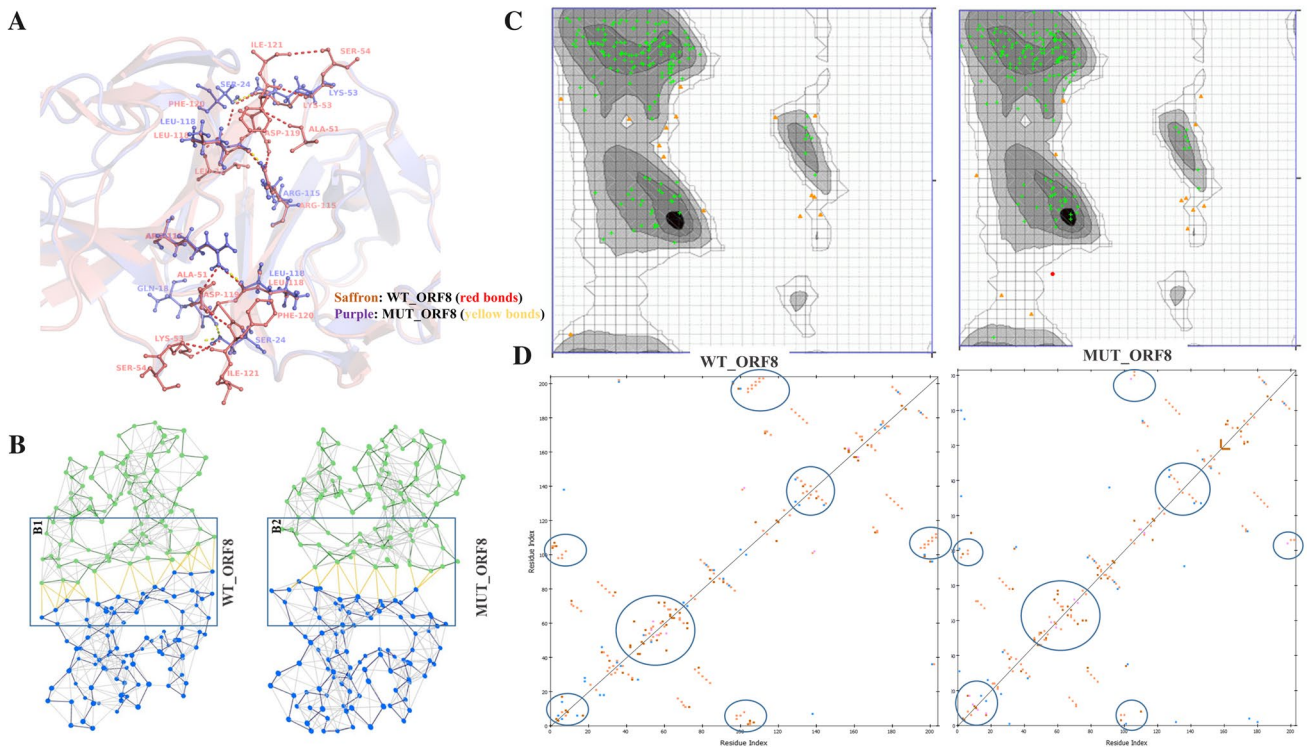

Fig. 1 Change in bond formation within WT_ORF8 and MUT_ORF8 due to 119Asp and 120F deletion: **A:** Superimposition of WT_ORF8 shown in saffron color and MUT_ORF8 shown in purple color. Hydrogen bond formation within two monomeric units of ORF8 is illustrated that using Pymol were red and yellow bonds representing bond formation within WT_ORF8 and MUT_ORF8. **B:** A network analysis of protein structures using NASP sever, where B1 and B2 represent network between dots as a node (amino acids) and inter and intramolecular bonds as an edge (yellow) for WT_ORF8 and MUT_ORF8, respectively. WT_ORF8 possesses 203 nodes and 722 edges while MUT_ORF8 possesses 202 nodes and 714 edges. **C:** Ramachandran plot for WT_ORF8 and MUT_ORF8. Green dots represent highly preferred observations, yellow dots represent preferred observations, and red dots represent questionable observations. MUT_ORF8 possesses two questionable observations which are C: E-64 and D: S-67, while WT_ORF8 possess no such kind of observations. **D:** Contact plot showing amino-acids contacts between monomeric units of WT_ORF8 and MUT_ORF8. Blue color shows main chain-side chain interactions, Saffron color shows main chain-main chain interactions, and brown color shows side chain-side chain interactions within monomeric subunits

MUT_ORF with lower interactions. Overall structural studies of ORF8 proteins suggesting that WT-ORF8 is a stable dimeric structure as compared to MUT_ORF8 through strong molecular interactions like hydrogen bonds and salt bridges between its monomeric units. These observations were further also confirmed using the molecular dynamics approach.

Molecular dynamics reveals breakdown/dissociation of ORF8 dimer in delta variant

After execution of the classical molecular dynamics simulations for 200 ns, the root mean square deviation (RMSD) of the trajectories were monitored, to identify the region of WT_ORF8 and MUT_ORF8 dimers showing deviations concerning the initial structure. Monitoring trajectories of ORF8 proteins would provide a better understanding of conformational aspects of ORF8 dimers. The RMSD plot showed that the conformational stability of WT_ORF8 is greater as compared to MUT_ORF8 (Fig. 2C). The RMSD of the MUT_ORF8 dimer is higher side throughout the simulation run time as compared to its initial conformations. The RMSD of WT_ORF8 has fluctuations between 1.733 ± 0.29 to 4.663 ± 0.29 Å throughout the simulation runtime of 0-200 ns. Whereas RMSD of the MUT_ORF8 is fluctuating from 1.88 ± 0.21 Å to 13.532 ± 0.17 Å during 0-200 ns. These increase in RMSD showing highly disordered behavior of MUT_ORF8 dimer in the system. The number of H-bonds were plotted for the duration of 0-200 ns simulation time (Fig. 2D). H-bond plot showed that WT_ORF8 has large number of H-bonds between 3–22 throughout the simulation. The maximum number of bonds is 22, formed at 102 ns simulation time in WT_ORF8. The number of H-bonds were also calculated for MUT_ORF8, varying from 0 to 15. The radius of gyration were studied to see the compactness of the protein structure of WT_ORF8 and MUT_ORF8. Δ119Asp and Δ120Phe were not favoring dimer formation in ORF8 which is seen during

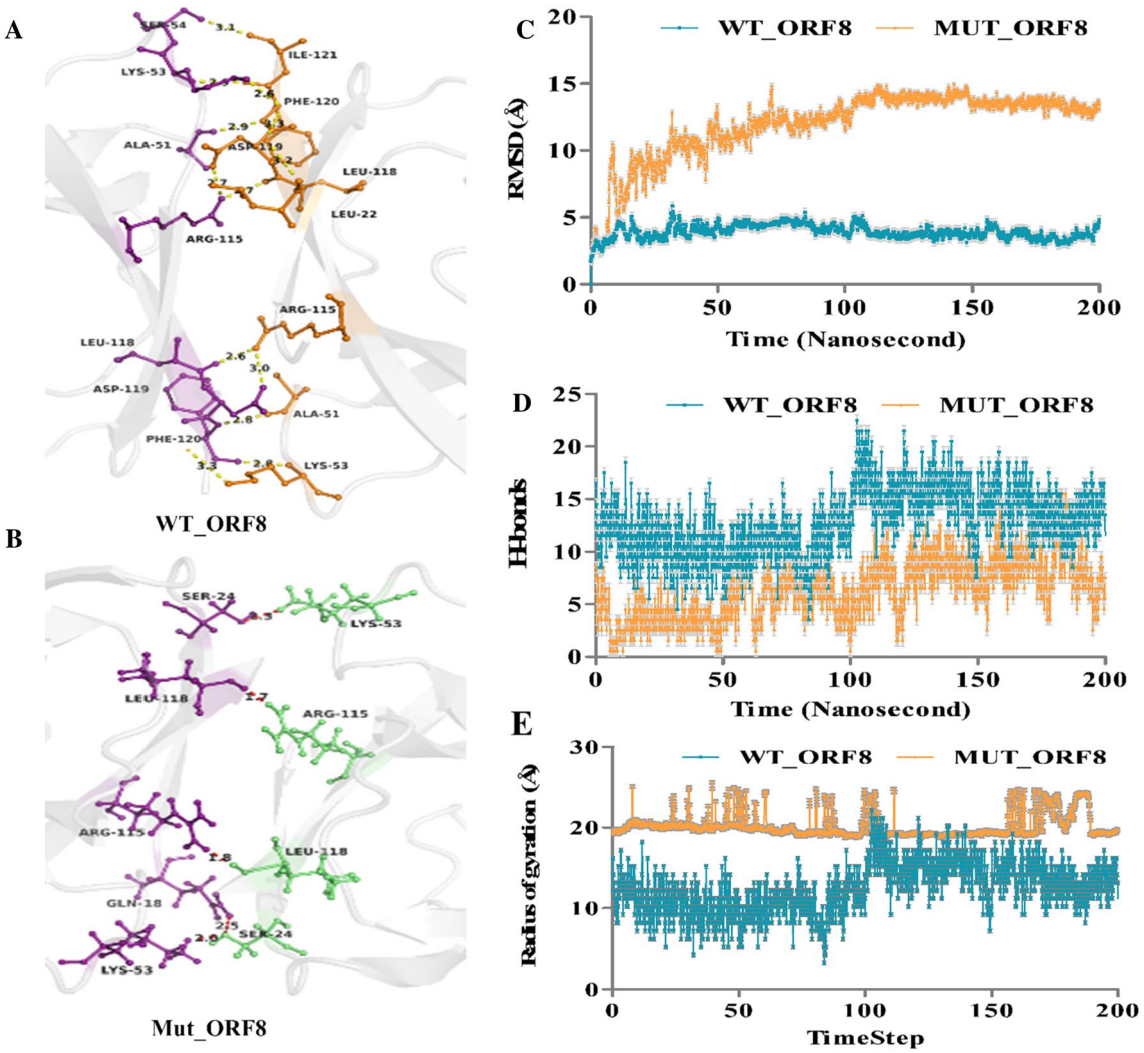

Fig. 2 Molecular dynamics studies for both variants of ORF8 dimer. **A** Intramolecular interactions between WT_ORF8 monomeric subunits **B** Intramolecular interactions between MUT_ORF8 monomeric subunits. **C** RMSD (root mean square deviation) within WT-ORF8(cyan) and MUT_ORF8 (orange) complex. **D** Hydrogen bonds formation within WT-ORF8(cyan) and MUT_ORF8 (orange) complex. **E:** Radius of gyration for WT-ORF8(cyan) and MUT_ORF8 (orange) complex

simulation, Supplementary video 2 shows the dissociation/breakdown of ORF8 monomers in mutant ORF8. In wild-type ORF8, such breakdown was not observed (Supplementary video 1). The highest radius of gyration of MUT_ORF8 throughout the simulation time, suggesting a less tight packing of MUT_ORF8 as compared to WT_ORF8 (Fig. 2E). The value of the radius of gyration is ranging from 16.175 ± 0.237–24.275 ± 0.147 Å in WT_ORF8 whereas, from 19.242 ± 0.243 to 22.175 ± 0.737-in MUT_ORF8. To investigate the effect of mutation on the dynamics of the backbone atoms, RMSF values for each dimer were calculated at each time point of the trajectories. Root mean square fluctuation (RMSF) values of WT_ORF8 are shifting from 0.831 ± 0.047 to 14.56 ± 0.071 Å. Only Residues 67, 68, 69, and 70 of WT_ORF8 are having a high RMSF values till 14.56 ± 0.071 Å, whereas other residues showing less RMSF value (Fig. 3A). RMSF values for MUT_ORF8 dimer is 1.3 to 7.078 Å, it is on the higher side throughout simulation as compared to WT_ORF8. Porcupine plots showing dynamics motions were also correlating with RMSF values. In Fig. 3B, section B1 box having higher dynamic motions with longer arrow length, while in section B2 both distance among MUT_ORF8 dimers seems to have increased compare to WT_ORF8. Distantly apart from geometry is showing possible case of dimer breakdown in MUT_ORF8. Dynamics cross-correlation matrix (DCCM) of WT_ORF8 and MUT_ORF8 were also plotted (Fig. 3C, D) In DCCM WT_ORF8, holding higher intensity for blue color as compared to MUT_ORF8. Positive Cij values signaling blue colors lead to improved interaction profile between residues.

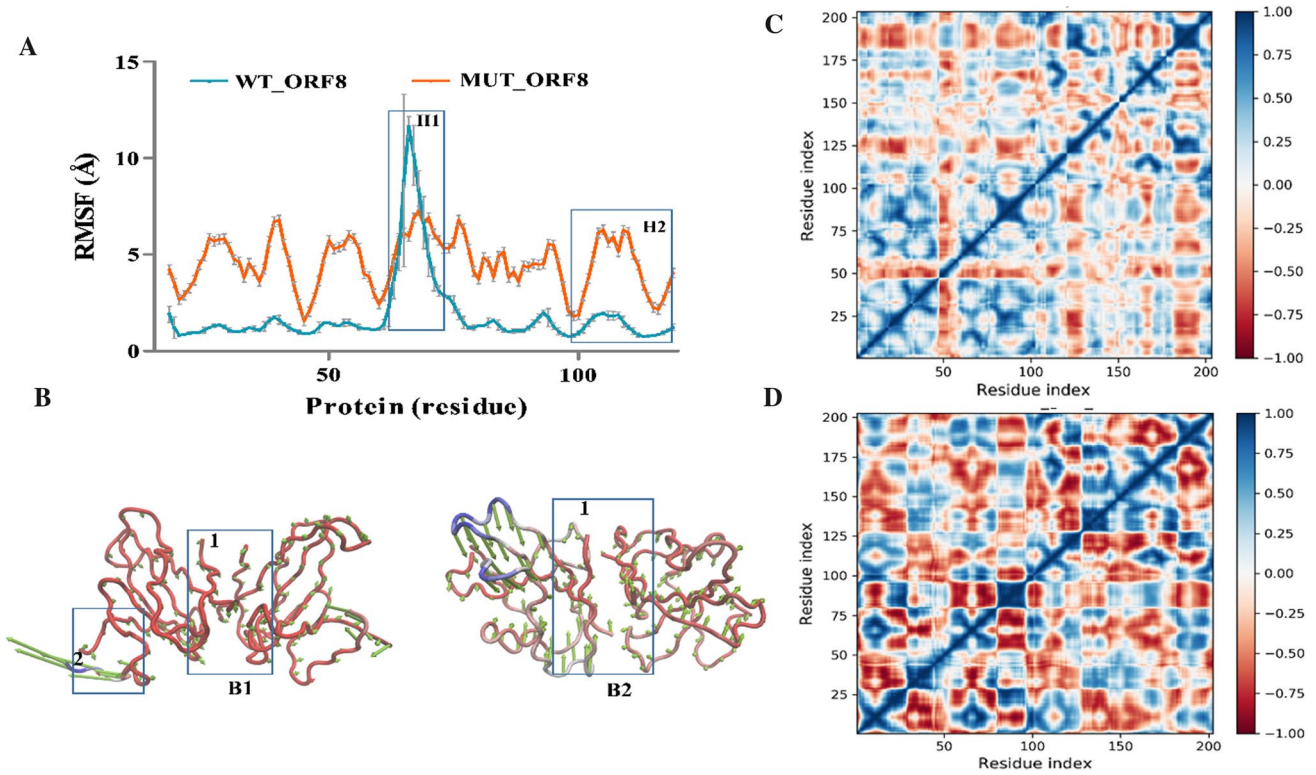

Fig. 3 Highly fluctuating motions in ORF8 dimers and Dynamic cross-correlation matrix **A** RMSF (root mean square fluctuation) in WT-ORF8 (cyan) and MUT_ORF8 (orange) complex. **B1** PCA1 mode of WT-ORF8, length of the arrow is in a linear relation between protein dynamics/fluctuation during trajectories blue color shows highly dynamic regions, while red color shows fewer dynamics regions. **B2** PCA1 mode of MUT-ORF8. **3C** and **2D** Dynamics cross-correlation matrix obtained from trajectories of WT_ORF8 and MUT_ORF8 complexes, respectively. The Blue to red color represents the c_{ij} values between 1 to -1. No cross-correlation was shown by white color

The binding energy (MMGBSA) calculations were performed for both dimers WT_ORF8 and MUT_ORF8. From Fig. 4A, it is clearly seen that WT_ORF8_wt is more stable having higher negative free energy as compared to MUT_ORF8. The electrostatic energy of WT_ORF8 and MUT_ORF8 was -295.08 ± 0.98 and -97.27 ± 0.56, respectively. A similar pattern has been observed for ΔG bind, Vander Waal energy, H-bond energy, lipophilic energy, covalent energy, and solvation energy for WT_ORF8 and MUT_ORF8 (Fig. 4A). It is evident that only three amino acids i.e., Arg115, Val117, and Ile121 are involved in dimerization of MUT_ORF8 as compared to WT_ORF8 where Val114, Arg115, Val116, Val117, Lue118, Asp119, Phe120, and Ile121 are involved in the stabilization of the WT_ORF8 dimer (Fig. 4C). Electrostatic potential is major energies that were contributing in dimer formation. Energies were visualized in the ABPS module implemented in Pymol 1.8. As shown in Fig. 4B, WT_ORF8 has a higher opposite attraction (positive–negative) compare to MUT_ORF8. Box B1 and B2 show the region where these electrostatic potentials persist for both variants. Increased electrostatic potential among amino acids of WT_ORF8 shows favorable dimer formation compared to MUT_ORF8. Energy minimized dimers obtained through MMGBSA were subjected to monomer interactions. From Fig. 4D, F, it is depicted that WT-ORF8 have 16 combined hydrogen bonds and salt bridges while MUT_ORF8 had only 8. Minimized dimeric structure of MUT_ORF8 showed, difference of twofold in bond formation. These results indicate that Mutant ORF 8 is losing its dimer forming capacity which might affects the virus infectivity in the host.

Flexible docking between Variants of ORF8 and MHC-I complex

As the binding interface between ORF8 and MHC-I is not known yet, thus we used flexible docking to study the molecular interactions between ORF8 and MHC-I using PIPER. As shown in Fig. 5A, the superimposed structure of docked pose of ORF8 and MHC-I was shown. Maximum possess were generated, showing binding of ORF8 between beta macroglobulin chain and alpha 3 domain of MHC-I, where both dimers of ORF8 can easily accommodate. Pivotal interactions among WT_ORF8 concerning MHC-I complex

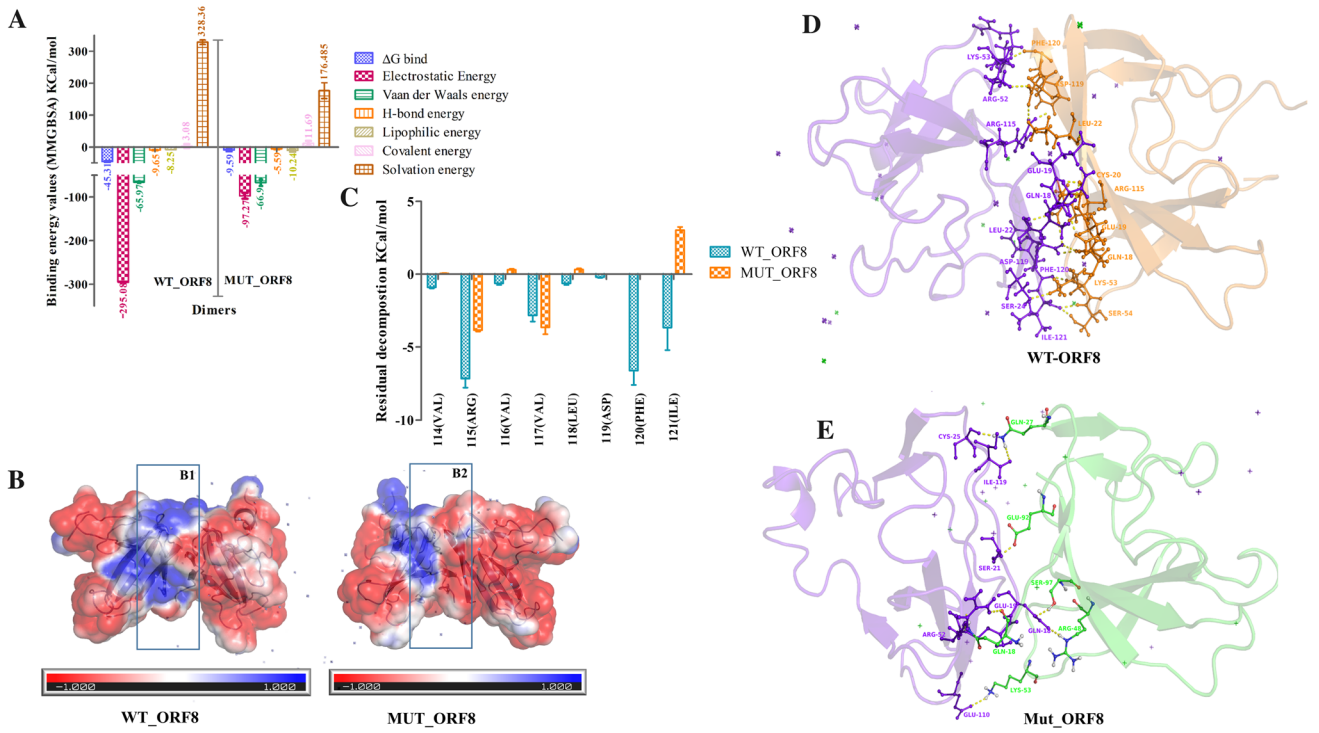

Fig. 4 Binding energy studies within dimers of ORF8. **A** Binding energy difference between WT_ORF8 and MUT_ORF8. Major energies involved in dimer formation are shown in different legends. **B** electrostatic interaction map drawn for 1st energy minimized dimer obtained from MMGBSA approach. Blue, white, and red colors represent positive, null, negative electrostatic potential, respectively, in form of surface representations. B1 & B2 represent potential between two monomeric subunits of WT-ORF8 and MUT-ORF8, respectively. **C** Thermal decomposition among amino-acids residues within both dimers. WT_ORF8 (cyan) and MUT_ORF8 (Orange) showing decomposition energies for key residues involved in dimer formations. **D** , **E** Interactions among energy minimized dimers obtained through MMGBSA, legends for each type of bond is shown in under Fig. 3E. Yellow dashes were hydrogen bonds formation within amino acids ball and stick conformation between monomers of ORF8

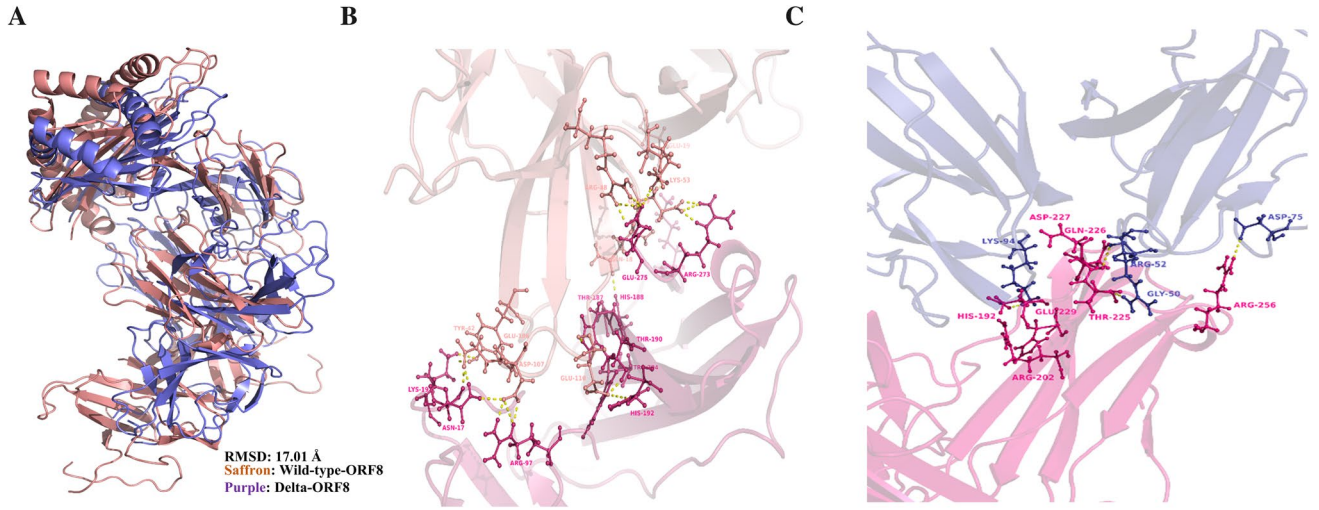

Fig. 5 Flexible docking of MHC-I with ORF8 dimer. **A** Superimposed structure of WT_ORF8_MHC-I (saffron) and MUT_ORF8_MHC-I (purple). **B** Pivotal interaction among WT_ORF8_MHC-I complex. **C** Pivotal interaction among MUT_ORF8_MHC-I complex. Saffron is wild-type ORF8, Purple is delta ORF8, and warm pink is MHC-1 complex. Hydrogen bonds between ORF8 and MHC-1 complex are shown in yellow dashes

are 18, and MUT_ORF8 concerning MHC-I were only 11 (Fig. 5B, C). Based on docking results, we hypothesized that the unstable dimeric structure of ORF8 (MUT_ORF8) might not be able to bind efficiently to the MHC-I complex, hence not able to capture it tightly for autophagy. These correlations further lead to enhance expression of MHC-I compared to wild-type virus infection.

Discussion

The molecular mechanism behind the severity and rapid spread of the Coronavirus disease is yet to be investigated. It is reported that ORF8 is a rapidly evolving dimeric protein that interferes with the immune responses in a host [12]. Some reports are showing that ORF8 is interacting with proteins such as IL17RA of the MHC-I molecular pathway [21]. It was also reported that SARS-CoV-2 virus infection leads to downregulation of MHC-I through direct interactions with ORF8 and is selectively targeted toward lysosomal autophagy, consequently immune evasion [43]. The antigen presentation system of the host will also be impaired due to ORF8-MHC-I interactions. MHC-1 complex is majorly involved in expression of viral antigenic peptides using cytotoxic pathway to host immune system, resulting in better immunity. ORF8 interects with MHC-1 and hence block its antigen presentation, hence suppressed immune response. If dimer of ORF8 is weaken which can results normal expression of MHC-1, hence prolonged immune response. Therefore, ORF8 has now become a prime target for the scientist to investigate the mechanism behind ORF8-MHC-I interactions. During the second wave of Coronavirus disease, although the infection rate was very high, it was seen that hosts developed adaptability toward the COVID-19 infection [5]. Therefore, the study was planned with two objectives firstly, exhaustive analysis of the molecular structures of ORF8 dimer of wild type and delta variant (WT_ORF8 and MUT_ORF8) and secondly the interactions between WT_ORF8-MHC-I complex and MUT_ORF8-MHC-I complex. The detailed analysis of dimeric structures of WT_ORF8 and MUT_ORF8 showed a significant difference in interaction patterns between the monomeric chains. In WT_ORF8, the key interaction is formed between Asp119 and Phe120 (Fig. 1C). Whereas, due to the deletion of Asp119 and Phe120 amino acids in MUT_ORF8 the interactions between MUT_ORF8 monomeric chains were diluted (Fig. 1A). Deletion of Asp119 and Phe120 in MUT_ORF8 protein of SARS CoV2 delta variant caused loss of three salt bridges as well as H-bonds. The structural instability of the MUT_ORF8 can be witnessed through molecular dynamics simulation studies. In MD studies, RMSD, RMSF and the radius of gyration of MUT_ORF8 are always toward the higher side as compared to WT_ORF8 (Fig. 2B, C and D). Reports are reported showing higher RMSD, RMSF, and Radius of gyration values leads to instability of complexes [1, 11, 39]. It was also observed at many time points of simulation the number of hydrogen bonds tends to zero in MUT_ORF8 indicating that there was the loss of connectivity between the monomeric chains of MUT_ORF8 (Fig. 2D). But in WT_ORF8 there are constant interactions between the monomeric chains revealing the conformational stability of the dimeric structure. Higher RMSF values for MUT_ORF8 dimer throughout simulation indicate greater flexibility. Additionally, the radius of gyration was also calculated for ORF8_WT and MUT_ORF8 dimers to study the compactness of these dimeric structures with protein folding and unfolding over thermodynamic principles during the 200 ns of the molecular dynamics simulation. It is evident that only three amino acids i.e., In MUT_ORF8, amino acids Arg115, Ile119, Ala51, Ser24 are involved in bond formation between the dimers, whereas Phe120 and Lys53, Lys53 and Ser24, Gln18-Lue22, Arg52 and Ile121 in addition to A: Asp119-B: Arg115, A: ARG115-B: Glu92, B: Asp119-A: Arg115 and B: Arg115-A: Glu92 are involved in the stabilization of the WT_ORF8. Interestingly, in addition to these interaction two pi-Sulfur bonds were also observed between A: Phe120-B: Cys90 and A: Phe120-B: Cys25 in WT_ORF8, which is totally absent in MUT_ORF8 due to deletion of Phe120 amino acid. As Ala51 and Ser24 are major interacting amino acid in case of MUT_ORF8 its detail interaction map was built that surprisingly showed that it is these two amino acids are forming unfavorable bonds i.e., D: Ala51-D: Ser97 and C: Ser24-D: Lys53, which is also contributing toward instability of MUT_ORF8.

The stability of ORF8 dimers seems to be one of the major reasons contributing toward the host immune adaptability because the stable dimeric protein WT_ORF8 can tightly accommodate on the surface of the MHC-I complex, whereas MUT_ORF8 is unable to firmly accommodate on the surface of the MHC-I complex causing escape of MHC-I complex toward lysosomal autophagy and contributing consequently in an increased immune response.

The authors attempted to link the loss of ORF 8 dimerization capacity to the host immune response in this study. As previously discussed, ORF-8 physically binds the MHC-1 complex to block the ER-Golgi mediated membrane trafficking pathway, resulting in MHC-1 downregulation in the host [43]. If ORF8 becomes weak, it will no longer be able to bind with MHC-1, and thus, MHC-1 expression will return to normal levels. The ICMR (Indian Council of Medical Research) conducted a nationwide population weighted study of seroprevalence from May to June 2020, revealing 0.75 percent among 21 states (Fig. 5C) [29]. In August 2020, a second seroprevalence study using an Abbott assay to detect IGg antibodies against SARS-CoV-2 nucleoprotein revealed an increase in seroprevalence to 6.6 percent (95

percent CI 58%–74%) [18]. Seroprevalence among adults in India increased by about tenfold, from 7% in May 2020 to 71% in August 2020 [26]. Supplementary Fig. 3A, showing the number of SARS-CoV-2 cases reported in India during the first and second waves. Third seroprevalence data show a percentage increase to 24.1% from December 2020 to January 2021 (Supplementary Fig. 3B). Dropdown of 50% cases SARS-CoV-2 cases during the second wave was double-quick time compared to the first wave (https://timesofindia.indiatimes.com/83074542). During the first wave on 17th September 2020, cases were 93,735, and cases were halved in 6 weeks, 30th October 2020 with 46,380 cases (Supplementary Fig. 3C). While in the second wave higher number of cases (3, 91,261) were decreased (1, 95,183) in half time compared to the first wave. ICMR 4th seroprevalence data show 70% of the Indian population (unvaccinated) showing IgG antibody titer against SARS-CoV-2 cases [30, 35]. A drastic increase in seroprevalence after the second wave, from 0.75% to 70% is an unusual observation for a high transmittable delta variant. Delta variant has these D119, F120 deletions, which were disrupting ORF8, responsible for downregulating MHC-I and suppressing host immune response. Figure 5A and B shows SARS-CoV-2 sequences submitted during 1st and 2nd wave. The red color is narrating sequences from delta variant. Frequency of delta is started increasing from March 2021, hence seroprevalence also. Results of the study suggest that the dimerization of MUT_ORF8 is altered, which might be affecting the ORF8 mediated MHC-I downregulation by autophagy in delta variant.

To support this nationwide study, state-wise seroprevalence was also studied in a region like Ahmedabad, Gujarat having a higher number of active cases of SARS-CoV-2 infection. Figure 6A shows genome sequencing data of SARS-CoV-2 from all over the India. Fig. 6B shows the genome sequencing data of the Gujarat biotechnology research center during the second wave, where B.1.167.2 (red) lineage (delta) was found to be 100% in samples collected from patients [16]. Seroprevalence of nationwide study during delta virus is 69%, and state wide is 90%. Nationwide frequency of delta is lower than Gujrat state wide frequency. This correlation is again supporting that delta with orf8 mutation might lead to higher seroprevalence. 5th seroprevalence data of Ahmedabad city are shown in Supplementary figure S4B. Seroprevalence due to delta only was 81.93% (Ahemdabad Summary, 2021). We had hypothesized that altered dimer of ORF8 might not able to perform autophagy of MHC-I molecule compared to

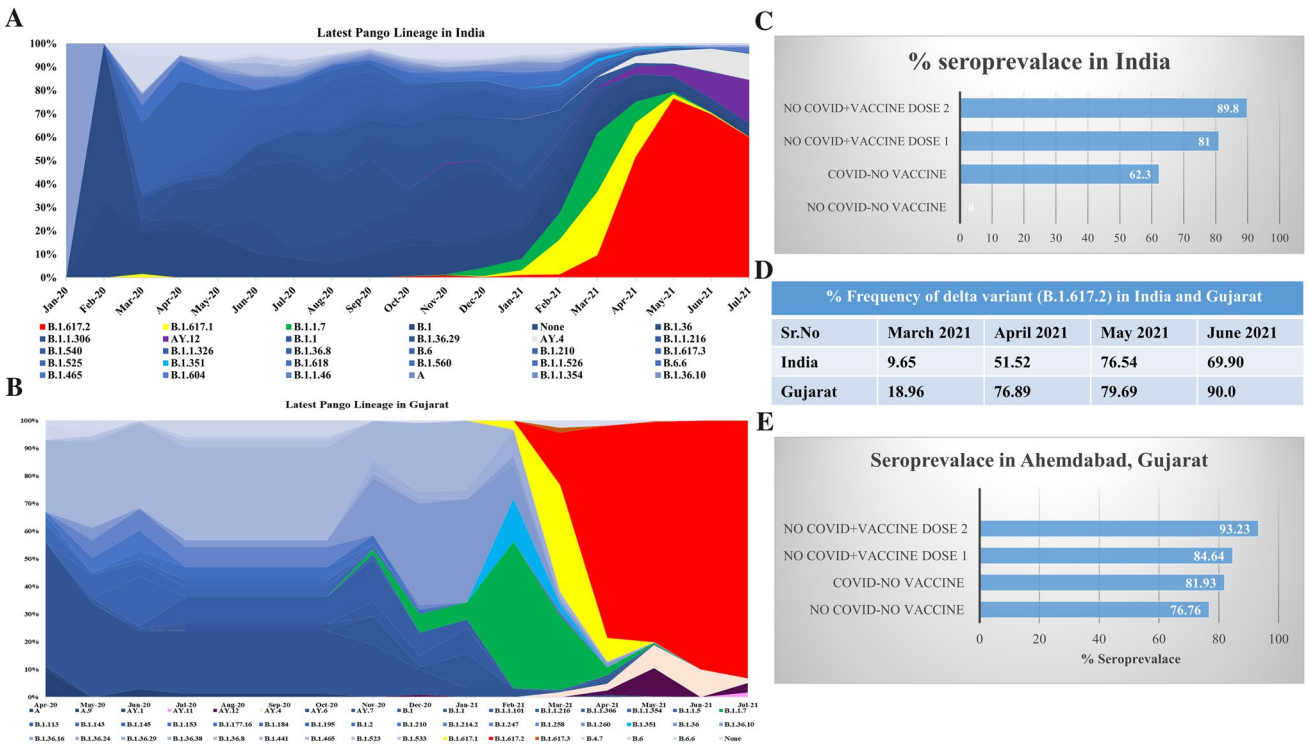

Fig. 6 Nationwide and statewide seroprevalence study: **A:** SARS-CoV-2 sequences submitted to GAISAD database from India at different time scale with latest Pango lineage. **B:** SARS-CoV-2 sequences submitted to GAISAD database from Gujarat at different time scale with latest Pango lineage. **C:** 5th Seroprevalence data from ICMR (Indian council of medical research). **D:** Table narrating frequency of delta variant (B.1.617.2) during the second wave in India and Gujarat. **E:** 5th Seroprevalence data from Ahmedabad city, Gujarat

wild-type ORF8, which might lead to favoring host immune responses. This can be one possible reason for the sudden drop down of cases during the second wave in India.

Materials and methods

Data retrieval

Crystal structure of ORF8 (PDB ID: 7JTL) protein of SARS-CoV-2 (WT_ORF8) was retrieved from protein data bank [12]. Protein sequence ORF8_GBRC_NCD_370 of SARS-CoV-2 delta variant (MUT_ORF8) was obtained from in-house sequencing (Sequence submitted to GISAID with accession number EPI_ISL_2001211) and fasta sequence of MHC-I protein (Accession no: NP_005505.2) was downloaded from NCBI.

Protein structure modeling and molecular dynamics simulations studies

3-Dimensional structures of MUT_ORF8 protein as well as of MHC-I protein were built using a homology modeling panel under the Schrodinger suite release 2021–2 [23]. The fasta sequences of MUT_ORF8 and MHC-I protein were imported into the Schrodinger suite. Homology blast search resulted in the templates 7JTL and 6AT5 corresponding to MUT_ORF8 and MHC-I, respectively. Protein preparation wizard was then used for the refinement of above protein structures. Additionally, the PRIME module was also used to add missing residues, and pKa refinement of proteins was done using an epic module of the Schrodinger suite [32].

Conformational stability of WT_ORF8 and MUT_ORF8 dimers were inspected using molecular dynamic simulations studies in detail using DESMOND module implemented in Schrodinger suite 2021–1 till 200 ns (ns)[48]. The OPLS4 force field was applied to refine the WT_ORF8 and MUT_ORF8 dimeric proteins, as well as H-bonds, were refilled using structure refinement panel implemented in Schrodinger suite [34, 47]. The particle mesh Ewald method was applied for the calculation of long-range electrostatic interactions [36]. Also, at every 1.2 ps interval the trajectories were recorded for the analysis. The proteins WT_ORF8 and MUT_ORF8 were placed in the center of the dodecahedron water box of the TIP3P water model of size wild 353968 Å and 360038 Å, respectively [45]. The whole system was neutralized using 1.5 mM salt concentration. A coupling constant of 2.0 ps under the Martyna–Tuckerman–Klein chain-coupling scheme was used for pressure control, and the Nosé–Hoover chain-coupling scheme at 310.3 K was used for temperature control of the system [24]. The whole system was initially energy minimized by steepest descent minimization. Total negative charges on the protein structures of WT_ORF8 and MUT_ORF8 were balanced by an appropriate number of Na + ions to make the whole system neutral. All molecular dynamics simulations were performed in triplicates till 200 ns. The binding energy of the system was calculated for each of the protein structures, and stability of the complex was monitored by analyzing RMSD, RMSF, the radius of gyration, and H-bonds of each dimer throughout simulation run time. High-resolution images were generated using Pymol and biovia Discovery studio [4, 31]. Protein networking was studied into NASP server available online [6]. Ramachandran plots were generated into zlab Ramachandran plot server [2].

Binding energy (MMGBSA) calculation

The binding free energy of WT_ORF8 and MUT_ORF8 dimers were calculated by Prime Molecular Mechanics-Generalized Born Surface Area (MMGBSA) using thermal_mmgbsa.py implemented under PRIME module of Schrodinger suite [3, 15, 22]. The binding free energy of each protein provides a summary of the biomolecular interactions between monomeric chains of protein dimer. OPLS4 force field and VSEB solvation models were used for MMGBSA calculation. The binding energy includes potential energy, as well as polar and non-polar solvation energies, were calculated as following.

$$\Delta G_{\text{Bind}} = \Delta G_{\text{SA}} + \Delta G_{\text{Solv}} + \Delta E_{\text{MM}}$$

Principal component analysis (PCA) and dynamics cross-correlation matrix (DCCM) calculation

To perform PCA, Primarily the covariance matrix C was calculated. The eigenvectors and eigenvalues were obtained for the covariance matrix C [19]. The elements Cij in the matrix C are defined as:

$$C_{ij} = \langle (r_i - \langle r_i \rangle) * (r_j - \langle r_j \rangle) \rangle \quad (1)$$

From Eq. 1, ri and rj are the instant coordinates of the ith or jth atom, $\langle r_i \rangle$ and $\langle r_j \rangle$ and mean the average coordinate of the ith or jth atom over the ensemble.

Correlative and anti-correlative motions are playing a key role in the recognition as well as binding in the biological-complex system. These motions can be prevailed through molecular dynamics simulation trajectories by defining the covariance matrix about atomic fluctuation. The magnitude of correlative motions of two residues can be represented by the cross-correlation coefficient, Cij. It is defined by the following equation:

$$C_{ij} = \frac{\langle \Delta r_{i*} \Delta r_j \rangle}{(\langle \Delta r_i \rangle^2 \langle \Delta r_j \rangle^2)^{1/2}} \quad (2)$$

Here i (j) is ith (jth) two residues (or two atoms/proteins), Δri (Δrj) is the displacement vector corresponding to ith (jth) two residues (or two atoms/proteins), and ⟨..⟩ is for the ensemble average. The value of Cij ranges from + 1 to -1. + Cij denotes positive correlation movement (same direction) shown in blue color, and -Cij denotes anti-correlation movement (opposite direction) shown in red color. The higher the absolute value of Cij is, the more correlated (or anti-correlated) the two residues (or two atoms or proteins). PCA and DCCM both were evaluated by using run trj_essential_dynamics.*py*, a python script under Desmond module of Schrodinger 2021–1 [7].

Conclusion

The frequency of delta variant during the second wave in India was persisted 9.6–76.5% in India while in Gujarat it was between 18.96 to 90% (Fig. 6D). 5th seroprevalence study by ICMR shows that 62.3% population have antibodies due to virus infection, while in Gujarat there 81.93% seroprevalence was observed. These patterns lead to conclude that as the frequency of delta is increasing seroprevalence among the population had also increased (Fig. 6C, D). This seroprevalence study supports our hypothesis that loss in dimerization capacity of ORF8 (from delta variant) leads to an abrogation of ORF8 MHC-I interaction and overcome the suppression of adaptive immune response.

Supplementary Information The online version contains supplementary material available at https://doi.org/10.1007/s11030-022-10405-9.

Authors contributions AC and IS performed Insilco experiments, Molecular dynamics, validated hypothesis, and wrote the manuscript. AP, MJ, and CJ provided funding, validated results, and corrected the manuscript.

Funding Funding is provided by Department of Science and Technology (DST) India.

Data availability Seroprevalence study was performed based on ICMR (Indian council of medical research), PIB (Press information bureau), Times of India (TOI), Gujarat Biotechnology research center's COVID19 portal (GBRC), MoHFW (Ministry of health and family welfare), Nextstrain and GISAID database. ICMR: https://www.icmr.gov.in/.PIB: https://pib.gov.in/PressReleseDetail.aspx?PRID=1748351. TOI: https://timesofindia.indiatimes.com/. GBRC: https://covid.gbrc.res.in/. MoHFW: https://www.mohfw.gov.in/. Nextstrain: https://nextstrain.org/ncov/gisaid/global. GISAID: https://www.gisaid.org/index.php?id=209

Declarations

Conflict of interest The authors declare that the research was conducted in the absence of any commercial or financial relationships that could be construed as a potential conflict of interest.

References

1. Al-Karmalawy AA, Dahab MA, Metwaly AM, Elhady SS, Elkaeed EB, Eissa IH, Darwish KM (2021) Molecular docking and dynamics simulation revealed the potential inhibitory activity of ACEIs against SARS-CoV-2 targeting the hACE2 receptor. Front Chem 9:227. https://doi.org/10.3389/fchem.2021.661230
2. Anderson RJ, Weng Z, Campbell RK, Jiang X (2005) Main-chain conformational tendencies of amino acids. proteins: structure. Funct Genet 60:679–689. https://doi.org/10.1002/prot.20530
3. Beard H, Cholleti A, Pearlman D, Sherman W, Loving KA (2013) applying physics-based scoring to calculate free energies of binding for single amino acid mutations in protein-protein complexes. PLOS One 8:1–11. https://doi.org/10.1371/journal.pone.0082849
4. BIOVIA, Dassault Systèmes, BIOVIA Workbook, Release 2020; BIOVIA Pipeline Pilot, Release 2020 SDDS No Title
5. Byambasuren O, Dobler CC, Bell K, Rojas DP, Clark J, McLaws ML, Glasziou P (2021) Comparison of seroprevalence of SARS-CoV-2 infections with cumulative and imputed COVID-19 cases: systematic review. PLoS ONE 16:1–14. https://doi.org/10.1371/journal.pone.0248946
6. Chakrabarty B, Parekh N (2016) NAPS: network analysis of protein structures. Nucleic Acids Res 44:W375–W382. https://doi.org/10.1093/nar/gkw383
7. Chang S, Hu J, Lin P, Jiao X, Tian X (2010) Substrate recognition and transport behavior analyses of amino acid antiporter with coarse-grained models. Mol BioSyst 6:2430–2438. https://doi.org/10.1039/c005266c
8. Chaudhari A, Chaudhari M, Mahera S, Saiyed Z, Nathani NM, Shukla S, Patel D, Patel C, Joshi M, Joshi CG (2021) In-Silico analysis reveals lower transcription efficiency of C241T variant of SARS-CoV-2 with host replication factors MADP1 and hnRNP-1. Inform Med Unlocked. https://doi.org/10.1016/j.imu.2021.100670
9. Chaudhari AM, Kumar D, Joshi M, Patel A, Joshi C (2021) E156G and Arg158, Phe-157/del mutation in NTD of spike protein in B.1.617.2 lineage of SARS-CoV-2 leads to immune evasion through antibody escape. bioRxiv. doi: https://doi.org/10.1101/2021.06.07.447321
10. Chi X, Yan R, Zhang J, Zhang G, Zhang Y, Hao M, Zhang Z, Fan P, Dong Y, Yang Y, Chen Z, Guo Y, Zhang J, Li Y, Song X, Chen Y, Xia L, Fu L, Hou L, Xu J, Yu C, Li J, Zhou Q, Chen W (2020) A neutralizing human antibody binds to the N-terminal domain of the Spike protein of SARS-CoV-2. Science 369:650–655. https://doi.org/10.1126/science.abc6952
11. Duan L, Guo X, Cong Y, Feng G, Li Y, Zhang JZH (2019) Accelerated molecular dynamics simulation for helical proteins folding in explicit water. Front Chem 7:540. https://doi.org/10.3389/fchem.2019.00540
12. Flower TG, Buffalo CZ, Hooy RM, Allaire M, Ren X, Hurley JH (2021) Structure of SARS-cov-2 ORF8, a rapidly evolving immune evasion protein. Proc Natl Acad Sci USA 118:1–6. https://doi.org/10.1073/pnas.2021785118
13. Fratev F (2020) The SARS-CoV-2 S1 spike protein mutation N501Y alters the protein interactions with both hACE2 and human derived antibody: A Free energy of perturbation study. bioRxiv 2020.12.23.424283. doi: https://doi.org/10.1101/2020.12.23.424283

14. Geng H, Subramanian S, Wu L, Bu H-F, Wang X, Du C, De Plaen IG, Tan X-D (2021) SARS-CoV-2 ORF8 forms intracellular aggregates and inhibits IFNγ-induced antiviral gene expression in human lung epithelial cells. Front Immunol 12:2108. https://doi.org/10.3389/fimmu.2021.679482
15. Greenidge PA, Kramer C, Mozziconacci JC, Wolf RM (2013) MM/GBSA binding energy prediction on the PDBbind data set: successes, failures, and directions for further improvement. J Chem Inf Model 53:201–209. https://doi.org/10.1021/ci300425v
16. Gujarat Biotechnology Research center, Gandhinagar G (2021) covid.gbrc.res.in
17. Jangra S, Ye C, Rathnasinghe R, Stadlbauer D, Alshammary H, Amoako AA, Awawda MH, Beach KF, Bermúdez-González MC, Chernet RL, Eaker LQ, Ferreri ED, Floda DL, Gleason CR, Kleiner G, Jurczyszak D, Matthews JC, Mendez WA, Mulder LCF, Russo KT, Salimbangon ABT, Saksena M, Shin AS, Sominsky LA, Srivastava K, Krammer F, Simon V, Martinez-Sobrido L, García-Sastre A, Schotsaert M (2021) SARS-CoV-2 spike E484K mutation reduces antibody neutralisation. Lancet Microbe. https://doi.org/10.1016/S2666-5247(21)00068-9
18. John J, Kang G (2021) Tracking SARS-CoV-2 infection in India with serology. Lancet Glob Health 9:e219–e220. https://doi.org/10.1016/S2214-109X(20)30546-5
19. Kormos BL, Baranger AM, Beveridge DL (2007) A study of collective atomic fluctuations and cooperativity in the U1A-RNA complex based on molecular dynamics simulations. J Struct Biol 157:500–513. https://doi.org/10.1016/j.jsb.2006.10.022
20. Lau EY, Negrete OA, Bennett WFD, Bennion BJ, Borucki M, Bourguet F, Epstein A, Franco M, Harmon B, He S, Jones D, Kim H, Kirshner D, Lao V, Lo J, McLoughlin K, Mosesso R, Murugesh DK, Saada EA, Segelke B, Stefan MA, Stevenson GA, Torres MW, Weilhammer DR, Wong S, Yang Y, Zemla A, Zhang X, Zhu F, Allen JE, Lightstone FC (2021) Discovery of small-molecule inhibitors of SARS-CoV-2 proteins using a computational and experimental pipeline. Front Mol Biosci 8:644. https://doi.org/10.3389/fmolb.2021.678701
21. Lin X, Fu B, Yin S, Li Z, Liu H, Zhang H, Xing N, Wang Y, Xue W, Xiong Y, Zhang S, Zhao Q, Xu S, Zhang J, Wang P, Nian W, Wang X, Wu H (2021) ORF contributes to cytokine storm during SARS-CoV-2 infection by activating IL-17 pathway. iScience 24:102293. https://doi.org/10.1016/j.isci.2021.102293
22. Lyne PD, Lamb ML, Saeh JC (2006) Accurate prediction of the relative potencies of members of a series of kinase inhibitors using molecular docking and MM-GBSA scoring. J Med Chem 49:4805–4808. https://doi.org/10.1021/jm060522a
23. Madhavi Sastry G, Adzhigirey M, Day T, Annabhimoju R, Sherman W (2013) Protein and ligand preparation: parameters, protocols, and influence on virtual screening enrichments. J Comput Aided Mol Des 27:221–234. https://doi.org/10.1007/s10822-013-9644-8
24. Martyna GJ, Klein ML, Tuckerman M (1992) Nosé-Hoover chains: The canonical ensemble via continuous dynamics. J Chem Phys 97:2635–2643. https://doi.org/10.1063/1.463940
25. McCallum M, De Marco A, Lempp FA, Tortorici MA, Pinto D, Walls AC, Beltramello M, Chen A, Liu Z, Zatta F, Zepeda S, di Iulio J, Bowen JE, Montiel-Ruiz M, Zhou J, Rosen LE, Bianchi S, Guarino B, Fregni CS, Abdelnabi R, Foo SYC, Rothlauf PW, Bloyet LM, Benigni F, Cameroni E, Neyts J, Riva A, Snell G, Telenti A, Whelan SPJ, Virgin HW, Corti D, Pizzuto MS, Veesler D (2021) N-terminal domain antigenic mapping reveals a site of vulnerability for SARS-CoV-2. Cell 184:2332-2347.e16. https://doi.org/10.1016/j.cell.2021.03.028
26. Murhekar MV, Bhatnagar T, Selvaraju S, Saravanakumar V, Thangaraj JWV, Shah N, Kumar MS, Rade K, Sabarinathan R, Asthana S, Balachandar R, Bangar SD, Bansal AK, Bhat J, Chopra V, Das D, Deb AK, Devi KR, Dwivedi GR, Khan SMS, Kumar CPG, Kumar MS, Laxmaiah A, Madhukar M, Mahapatra A, Mohanty SS, Rangaraju C, Turuk A, Baradwaj DK, Chahal AS, Debnath F, Haq I, Kalliath A, Kanungo S, Kshatri JS, Lakshmi GGJN, Mitra A, Nirmala AR, Prasad GV, Qurieshi MA, Sahay S, Sangwan RK, Sekar K, Shukla VK, Singh PK, Singh P, Singh R, Varma DS, Viramgami A, Panda S, Reddy DCS, Bhargava B, Andhalkar R, Chaudhury A, Deval H, Dhatrak S, Gupta RR, Ilayaperumal E, Jagjeevan B, Jha RC, Kiran K, Krishnan NN, Kumar A, Kumar VV, Nagbhushanam K, Nimmathota A, Pandey AK, Pawar HS, Rathore KS, Robinson A, Singh HB, Wilson VC, Yadav A, Yadav R, Karunakaran T, Pradhan J, Sivakumar T, Jose A, Kalaiyarasi K, Dasgupta S, Anusha R, Anand T, Babu GR, Chauhan H, Dikid T, Gangakhedkar RR, Kant S, Kulkarni S, Muliyil JP, Pandey RM, Sarkar S, Shrivastava A, Singh SK, Zodpey S, Das A, Das P, Dutta S, Kant R, Narain K, Narasimhaiah S, Pati S, Patil S, Rajkumar H, Ramarao T, Sarkar K, Singh S, Toteja GS, Zaman K (2021) SARS-CoV-2 antibody seroprevalence in India, August–September, 2020: findings from the second nationwide household serosurvey. Lancet Glob Health 9:e257–e266. https://doi.org/10.1016/S2214-109X(20)30544-1
27. Pereira F (2021) SARS-CoV-2 variants combining spike mutations and the absence of ORF8 may be more transmissible and require close monitoring. Biochem Biophys Res Commun 550:8–14. https://doi.org/10.1016/j.bbrc.2021.02.080
28. Rashid F, Dzakah EE, Wang H, Tang S (2021) The ORF8 protein of SARS-CoV-2 induced endoplasmic reticulum stress and mediated immune evasion by antagonizing production of interferon beta. Virus Res 296:198350. https://doi.org/10.1016/j.virusres.2021.198350
29. Res M, Ruts C, Hospital CR, Sciences M, Committee IE, Crh-smims S (2018) Prevalence of. 517–520. doi: https://doi.org/10.4103/ijmr.IJMR
30. Research ICOM https://pib.gov.in/PressReleasePage.aspx?PRID=1739902
31. Schrodinger, LLC. 2010. The PyMOL Molecular Graphics System V 1. . pymol
32. Shelley JC, Cholleti A, Frye LL, Greenwood JR, Timlin MR, Uchimaya M (2007) Epik: a software program for pKaprediction and protonation state generation for drug-like molecules. J Comput Aided Mol Des 21:681–691. https://doi.org/10.1007/s10822-007-9133-z
33. Soh WT, Liu Y, Nakayama EE, Ono C, Torii S, Nakagami H, Matsuura Y, Shioda T, Arase H (2020) The N-terminal domain of spike glycoprotein mediates SARS-CoV-2 infection by associating with L-SIGN and DC-SIGN. bioRxiv 1–30
34. Steinbrecher T, Abel R, Clark A, Friesner R (2017) Free energy perturbation calculations of the thermodynamics of protein side-chain mutations. J Mol Biol 429:923–929. https://doi.org/10.1016/j.jmb.2017.03.002
35. Summary E (2021) 5 th Serosurveillance study in Ahmedabad executive summary title : assessing population based seropositivity for antibodiES Aim : Objectives :
36. Toukmaji AY, Board JA (1996) Ewald summation techniques in perspective: a survey. Comput Phys Commun 95:73–92. https://doi.org/10.1016/0010-4655(96)00016-1
37. Vincent S, Arokiyaraj S, Saravanan M, Dhanraj M (2020) Molecular docking studies on the anti-viral effects of compounds from kabasura kudineer on SARS-CoV-2 3CLpro. Front Mol Biosci 7:434. https://doi.org/10.3389/fmolb.2020.613401
38. Vivekanandhan K, Shanmugam P, Barabadi H, Arumugam V, Daniel Paul Raj D, Sivasubramanian M, Ramasamy S, Anand K, Boomi P, Chandrasekaran B, Arokiyaraj S, Saravanan M (2021) Emerging therapeutic approaches to combat COVID-19: present status and future perspectives. Front Mol Biosci 8:55. https://doi.org/10.3389/fmolb.2021.604447

39. Wang J, Alekseenko A, Kozakov D, Miao Y (2019) Improved modeling of peptide-protein binding through global docking and accelerated molecular dynamics simulations. Front Mol Biosci 6:112. https://doi.org/10.3389/fmolb.2019.00112
40. Wordometer (2021) No Title. Worldometer COVID-19 coronavirus pandemic 2021; published online August
41. Yue J, Jin W, Yang H, Faulkner J, Song X, Qiu H, Teng M, Azadi P, Zhang F, Linhardt RJ, Wang L (2021) Heparan sulfate facilitates spike protein-Mediated SARS-CoV-2 host cell invasion and contributes to increased infection of SARS-CoV-2 G614 mutant and in lung cancer. Front Mol Biosci 8:292. https://doi.org/10.3389/fmolb.2021.649575
42. Zhang L, Jackson CB, Mou H, Ojha A, Peng H, Quinlan BD, Rangarajan ES, Pan A, Vanderheiden A, Suthar MS, Li W, Izard T, Rader C, Farzan M, Choe H (2020) SARS-CoV-2 spike-protein D614G mutation increases virion spike density and infectivity. Nat Commun 11:1–9. https://doi.org/10.1038/s41467-020-19808-4
43. Zhang Y, Chen Y, Li Y, Huang F, Luo B, Yuan Y, Xia B, Ma X, Yang T, Yu F, Liu J, Liu B, Song Z, Chen J, Yan S, Wu L, Pan T, Zhang X, Li R, Huang W, He X, Xiao F, Zhang J, Zhang H (2021) The ORF8 protein of SARS-CoV-2 mediates immune evasion through down-regulating MHC-I. Proc Natl Acad Sci. https://doi.org/10.1073/pnas.2024202118
44. Zhang Y, Zhang J, Chen Y, Luo B, Yuan Y, Huang F, Yang T, Yu F, Liu J, Liu B, Song Z, Chen J, Pan T, Zhang X, Li Y, Li R, Huang W, Xiao F, Zhang H (2020) The ORF8 protein of SARS-CoV-2 mediates immune evasion through potently downregulating MHC-I. bioRxiv. doi: https://doi.org/10.1101/2020.05.24.111823
45. Zielkiewicz J (2005) Structural properties of water: comparison of the SPC, SPCE, TIP4P, and TIP5P models of water. J Chem Phys. https://doi.org/10.1063/1.2018637
46. Zinzula L (2021) Lost in deletion: The enigmatic ORF8 protein of SARS-CoV-2. Biochem Biophys Res Commun 538:116–124. https://doi.org/10.1016/j.bbrc.2020.10.045
47. van Zundert GCP, Moriarty NW, Sobolev OV, Adams PD, Borrelli KW (2021) Macromolecular refinement of X-ray and cryoelectron microscopy structures with Phenix/OPLS3e for improved structure and ligand quality. Structure. https://doi.org/10.1016/j.str.2021.03.011
48. (2006) SC '06: Proceedings of the 2006 ACM/IEEE Conference on Supercomputing. Association for Computing Machinery, New York, NY, USA